Contents

List of Figures

List of Tables

1 Introduction

Micro electrical mechanical systems (MEMS) have been heavily researched, as the development of traditional piezo-based ultrasound imaging technology has reached its limit. Thus, novel high-resolution imaging methods, specifically pertaining to smaller objects, must be developed. Consequently, capacitive micro-machined ultrasound transducers (CMUT) have generated considerable interest as they exhibit distinguishing properties that current piezoelectric ultrasonic transducers lack [3]. Hence, as further research is performed regarding the fabrication and optimization of CMUT technology, it is required that the fundamental physical theory is well understood. Thus, it is important to have accurate analytical and numerical models of CMUT devices.

Herein this report, general background information pertaining to CMUT operation, the motivation of this project, and finally the methods and results are presented and discussed.

2 Background

2.1 Capacitive Micromachined Ultrasound Transducers

Ultrasound transducers convert electrical energy, such as an applied voltage bias, into mechanical energy, producing sound waves whose frequencies are above the human hearing threshold ($> 20kHz$). The ultrasound pulse will propagate through a given medium until it experiences a velocity fluctuation, indicating that it has interacted with a different material. This acoustic impedance mismatch will cause a portion of the ultrasound wave to reflect in a manner similar to light waves interacting with refractive index gradients. The reflected ultrasound beams are then detected by the emitting device, enabling the location of materialistic interfaces to be determined. This is accomplished via time of flight (TOF) analysis, in which the elapsed sent-received signal time is monitored.

A series of scan lines, each known as an A-scan, are used in order to acquire an ultrasound image. These scans are generated through the linear focusing of ultrasound waves. The sound velocity gradient is identified by analyzing the relative intensities of the incident and reflected signals. A series of A-scan acquisitions, performed at various angles, can be used in combination in order to produce a 2D image, which is typically referred to as a B-scan.

Beam focusing is achieved by beam forming, shown in Figure 1. Beam forming requires pulsed emission from numerous transducer elements with calculated delay periods, resulting in a highly focused beam.

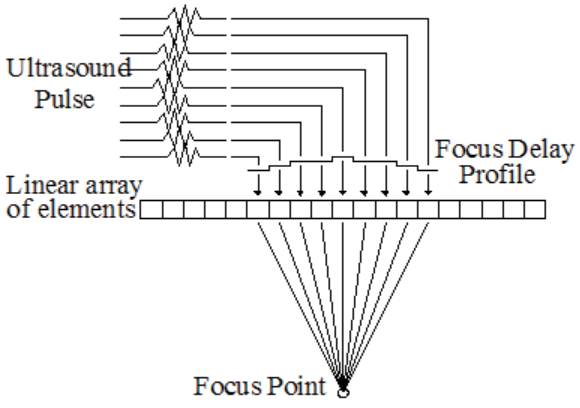

Figure 1: Controlling the focus point of an ultrasound pulse [1]

The operational mechanism of a CMUT differs from that of a traditional piezoelectric transducer. A CMUT generates an ultrasonic pulse by means of an applied voltage bias between

a capacitive plate and a thin capacitive membrane. The thin membrane is subsequently deflected due to the resulting, attractive electrostatic force. The subsequent application of a high-frequency AC voltage results in ultrasound pulses.

Similarly, in signal-receiving mode, the ultrasound-induced deflection profile results in a capacitance change. The received signal intensity, and hence resolution, can be maximized through the use of a compliant capacitive membrane. Within a CMUT design, this condition is satisfied by the application of a DC voltage, producing a strongly attractive force and thus reducing the relative displacement between both capacitors. Typically this bias is applied such that its magnitude is slightly less than the pull-in voltage, V_{PI}, of the capacitive plates, enabling the achievement of large amplitude gains with very small AC signals [2].

In order to elaborate upon this concept, consider a first-ordered lumped element model consisting of a capacitor, a mass, and a spring. The mass will actuate due to the resultant force of the capacitive and spring components of the design, which is described as

$$F_{cap} + F_{spring} = F_{mass}. \tag{1}$$

The force component of the capacitor, F_{cap}, is derived from the electrostatic force generated from the voltage bias,

$$F_{cap} = -\frac{d}{dx}\left(\frac{1}{2}CV^2\right) = \frac{\epsilon_0 A V^2}{2(g_0 - w)^2}. \tag{2}$$

In the above equation, A corresponds to electrode area, g_0 represents the effective distance between capacitive plates, and w corresponds to the membrane displacement from its unbiased position. Additionally, F_{spring} is obtained from Hooke's law and F_{mass} from Newton's second law of motion.

Combining these terms into Equation 1, the following result is obtained:

$$m\frac{d^2x(t)}{dt^2} - \frac{\epsilon_0 A V(t)^2}{2(g_0 - w(t))^2} + kw(t) = 0. \tag{3}$$

For a static deflection, the force balance can be simplified to

$$\frac{\epsilon_0 A V^2}{2(g_0 - w)^2} = kw. \tag{4}$$

Evidently, as the applied voltage is increased, the static gap distance decreases, resulting in the increase of the spring force.

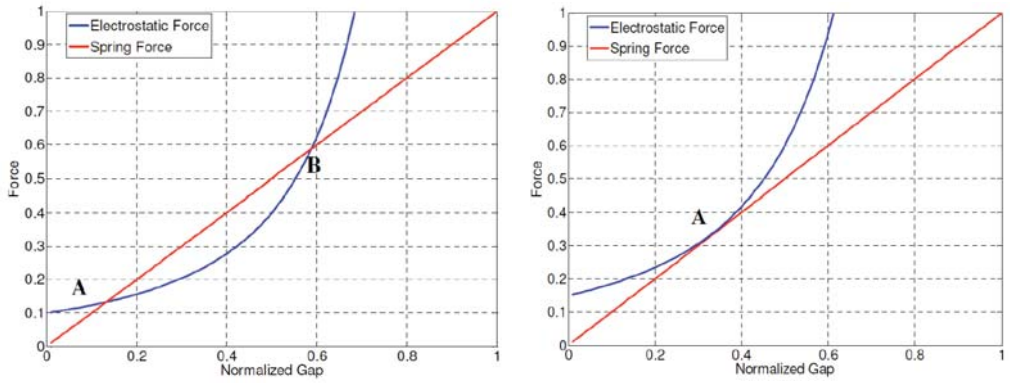

(a) $V < V_{pull-in}$ (b) $V = V_{pull-in}$

Figure 2: Resulting force as a function of gap distance, g [2]

Two mathematical solutions are available for the description of a CMUT that is operated at voltages lower than its pull-in voltage. These are shown in Figure 2a, in which Point B corresponds to an unstable solution - it will result in capacitive plate collapse due to the dominant electrostatic force [2]. The voltage at which this phenomenon occurs is referred to as the pull-in voltage of the system, displayed in Figure 2b. Conversely, at point A, the overpowering spring force will return the system to equilibrium.

2.2 Isotropic Silicon

Isotropic materials, such as amorphous silicon, are directionally independent and hence are not characterized in terms of specific crystal orientations. Consequently, their complete geometries are described by a single Young's modulus which is used in order to calculate the stress and strain acting upon the material. This is achieved using Hooke's law, shown in Equation 5.

$$\sigma = E\epsilon \tag{5}$$

In the above equation, σ corresponds to stress, ϵ corresponds to strain, and E corresponds to the Young's modulus of the material.

2.3 Anisotropic Silicon

Contrary to isotropic silicon, anisotropic silicon is directionally dependent. Consequently, compliance and stiffness tensors, each containing up to 36 terms, are required in order to obtain a complete description of the elasticity of the material. The resulting stresses and strains for [100] silicon are calculated from these matrices according to Equations 6 and 7 [4].

$$\begin{bmatrix}\sigma_1\\ \sigma_2\\ \sigma_3\\ \sigma_4\\ \sigma_5\\ \sigma_6\end{bmatrix} = \begin{bmatrix}165.6GPa & 63.9GPa & 63.9GPa & 0 & 0 & 0\\ 63.9GPa & 165.6GPa & 63.9GPa & 0 & 0 & 0\\ 63.9GPa & 63.9GPa & 165.6GPa & 0 & 0 & 0\\ 0 & 0 & 0 & 79.5GPa & 0 & 0\\ 0 & 0 & 0 & 0 & 79.5GPa & 0\\ 0 & 0 & 0 & 0 & 0 & 79.5GPa\end{bmatrix} \begin{bmatrix}\varepsilon_1\\ \varepsilon_2\\ \varepsilon_3\\ \varepsilon_4\\ \varepsilon_5\\ \varepsilon_6\end{bmatrix} \tag{6}$$

$$\begin{bmatrix}\varepsilon_1\\ \varepsilon_2\\ \varepsilon_3\\ \varepsilon_4\\ \varepsilon_5\\ \varepsilon_6\end{bmatrix} = \begin{bmatrix}7.68pPa & -2.14pPa & -2.14pPa & 0 & 0 & 0\\ -2.14pPa & 7.68pPa & -2.14pPa & 0 & 0 & 0\\ -2.14pPa & -2.14pPa & 7.68pPa & 0 & 0 & 0\\ 0 & 0 & 0 & 12.6pPa & 0 & 0\\ 0 & 0 & 0 & 0 & 12.6pPa & 0\\ 0 & 0 & 0 & 0 & 0 & 12.6pPa\end{bmatrix} \begin{bmatrix}\sigma_1\\ \sigma_2\\ \sigma_3\\ \sigma_4\\ \sigma_5\\ \sigma_6\end{bmatrix} \tag{7}$$

3 Fabrication

A single wafer, multi-step photo-lithography process is a common approach in the fabrication of CMUT devices [3]. The initial stage of such a process consists of the deposition and patterning of a sacrificial layer, typically either silicon nitride or silicon oxide, onto the silicon substrate. Next the capacitive CMUT membrane is deposited. A via is then created in order to allow the sacrificial layer to be etched and is subsequently sealed. Finally, a metallic electrode is patterned and deposited onto the substrate.

A second fabrication method is typically employed if the CMUT is to be used in an aqueous environment. This is to avoid the necessity of the via. The transducer cavity is created and is then bonded to a SOI (silicon-on-insulator) wafer in order to create a sealed membrane. The

sacrificial layer is then removed by etching the SOI wafer, resulting in a thin, uniform capacitive membrane. Finally, the metallic electrode is patterned and deposited onto the membrane of the device [5].

4 Objectives

The principal objective of this COMSOL finite element analysis is to determine which analytical model best matches the numerical deflection profile obtained for isotropic and anisotropic square CMUTs. An additional purpose is to determine the analytical peak deflections of each model in order to validate the CMUT design and boundary conditions within COMSOL; model validation is crucial as an accurate membrane deflection profile is essential for CMUT capacitance calculations, which are used in order to determine the pull-in voltage of the device. The complete deflection profile of each analytical model is then compared to that obtained from the FEM simulation. Lastly, conclusions pertaining to the analytical solutions that best match the FEA simulation models are drawn.

5 Analytical Solution

Analytical solutions for the deflection profiles of the various CMUT geometries are essential for model validation as well as to achieve the objective of this investigation. The general analytical plate deflection equation can be written as

$$\Delta p = \varrho h \ddot{w} + \nabla_{\perp}^2 D \nabla_{\perp}^2 w + \sigma_0 h \nabla_{\perp}^2 w. \tag{8}$$

In the above equation, ϱ represents the mass density of the plate, Δp is the applied pressure load, h corresponds to the height of the plate, σ_0 represents the pre-stress to which the plate is subjected, and w is the plate deflection along the z axis. Additionally, the two-dimensional Laplacian, $\nabla_{\perp}^2$, is given in Equation 9 whereas the flexural rigidity coefficient, D, is given in equation 10. Here ν corresponds to the Poisson ratio of the plate material.

$$\nabla_{\perp}^2 = \frac{\partial^2}{\partial x^2} + \frac{\partial^2}{\partial y^2} \tag{9}$$

$$D = \frac{Eh^3}{12(1-\nu^2)} \tag{10}$$

The square CMUT membrane considered in this investigation was not pre-stressed and hence the remainder of this report will consider the case in which σ_0 assumes a value of zero, reducing Equation 8 to

$$\Delta p = \varrho h \ddot{w} + \nabla_{\perp}^2 D \nabla_{\perp}^2 w. \tag{11}$$

Exact solutions to this plate equation have been found for circular membranes whereas only approximations can be obtained for square CMUT membranes.

5.1 Circular Plate Equation Solution

It has been well-documented that the deflection $w(r)$ of a circular membrane can be modelled by one of two equations based upon the geometry of the device [6, 7]. Equation 12a can be used to obtain the deflection profile of thin membranes - those membranes in which the peak deflection, w_0, is of greater magnitude than the membrane thickness h. Equation 12b can be used to obtain the deflection profile of thick membranes - those membranes in which the peak deflection is of lower magnitude than the membrane thickness. In these equations r corresponds

to the distance of a given point from the centre of the membrane whereas R represents the total plate radius.

$$w(r)_{thin} = w_0 \left[1 - \frac{r^2}{R^2}\right] \tag{12a}$$

$$w(r)_{thick} = w_0 \left[1 - \frac{r^2}{R^2}\right]^2 \tag{12b}$$

The analytical solution to the center deflection of a circular CMUT can then be written as follows [6, 7]

$$w_0 = \frac{\Delta p r^4}{64 D_i}, \tag{13}$$

where D_i is the isotropic flexural rigidity, defined in Equation 10.

Although such exact solutions do exist for circular and elliptical CMUT membranes and while they can be easily fabricated using modern process flow technologies, such design geometries are sub-optimal; the total surface area occupied by these devices relative to the total surface area of the consumed wafer is not maximized. A more efficient CMUT device would consist of square or hexagonal membranes.

5.2 Isotropic Square Plate

For the case of square and rectangular membranes, a closed form solution does not exist - the solution is an infinite Fourier series. Thus in order to extract an expression for the central, or maximal, deflection of square membranes, the shape membrane displacement profile must be inferred. The peak displacement can then be solved through the minimization of the total potential energy of the system, as shown in Equation 14 [7].

$$\frac{\partial U}{\partial \omega_0} = \frac{\partial}{\partial \omega_0}\left[\int\left\{\int\left[\frac{D_i}{2}\left(\nabla_\perp^2 w\right)^2 - p_0 w\right] dy\right\} dx\right] = 0. \tag{14}$$

This approach has led to peak displacement approximations for both macroscopic and microscopic square membranes.

5.2.1 Macroscopic Approximation to Membrane Displacement Profile

First, the macroscopic case is considered, in which the bending of thick membranes is dominated by bending moments. This solution is commonly found in classical mechanics textbooks [6]. This is obtained by assuming a parabolic deflection shape.

$$w(x, y) = w_0 \left(1 - \frac{x^2}{a^2}\right)\left(1 - \frac{y^2}{a^2}\right) \tag{15}$$

In the above approximation, x and y are the Cartesian displacements away from the centre of the membrane, w_0 is the centre deflection, and a represents half the length of a single side of the square membrane. The peak deflection can then be calculated as

$$w_0 = \frac{1}{792}\frac{(2a)^4}{D_i}\Delta p, \tag{16}$$

where D_i is the isotropic flexural rigidity described above.

5.2.2 Microscopic Approximation to Membrane Displacement Profile

The peak deflection of a microscopic square membrane can be obtained by inferring the following deflection profile [7]:

$$w(x,y) = \frac{w_0}{4}\left(1 + cos\frac{\pi x}{R}\right)\left(1 + cos\frac{\pi y}{R}\right). \tag{17}$$

Using this approach, the peak deflection of a square, isotropic CMUT membrane can be derived as

$$w_0 = \underbrace{\frac{1}{8\pi^4}}_{\approx 1/779.3}\frac{(2a)^4}{D_i}\Delta p. \tag{18}$$

5.2.3 Galerkin Method

Finally, a third deflection shape is approximated using the Galerkin method as described by Thomsen et al [8]. This assumed deflection profile is given by

$$w(x,y) = \sum_{k=0,1...}^{\infty}\sum_{l=0,1...}^{\infty}\alpha_{kl}\phi_{kl}(x,y). \tag{19}$$

For square plates the deflection shape is assumed to be

$$\phi_{kl}(x,y) = \left(a^2 - x^2\right)^2\left(a^2 - y^2\right)^2 x^k y^l, \tag{20}$$

which can be reduced to Equation 21, if only three terms are used in the expansion.

$$w(x,y) = \frac{77\Delta p(a^2 - x^2)^2(a^2 - y^2)^2(269a^2 + 72(x^2 + y^2))}{1025280 D_i a^6} \tag{21}$$

This approach yields a peak deflection approximation corresponding to

$$w_0 = \underbrace{\frac{20713}{16404480}}_{\approx 1/791.99}\frac{(2a)^4}{D_i}\Delta p. \tag{22}$$

5.3 Anisotropic Square Plate

An analytical approximation to the beam deflection profile of a square, clamped anisotropic membrane is available if the Galerkin method is used, in which the deflection profile is approximated by the series shown in Equation 19. The same deflection shape as the isotropic case is assumed. This approximation results in the following deflection profile:

$$w(x,y) = \left(a^2 - x^2\right)^2\left(a^2 - y^2\right)^2\sum_{k=0,1...}^{\infty}\sum_{l=0,1...}^{\infty}\alpha_{kl}x^k y^l. \tag{23}$$

For a single-term Galerkin expansion of a square, anisotropic membrane, the coefficient α_{00} is expressed as

$$\alpha_{00} = \frac{49\Delta p}{128(7a^4 + 2a^4 k_2 + 7a^4 k_4)D_a}. \tag{24}$$

In the above equation, D_a is the anisotropic flexural rigidity, which is defined in equation 25, and k_2 and k_4 correspond to the membrane coefficients which, for [100] silicon, reduce to equations 26 and 27.

$$D_a = \left(\frac{h^3}{12}\right)\left(\frac{-s_{11}s_{44}}{s_{11}(-s_{11}s_{44}) + s_{44}s_{12}^2}\right) \tag{25}$$

$$k_2 = 2\frac{2s_{11}^2 - 2s_{12}^2 - s_{44}s_{12}}{s_{11}s_{44}} \tag{26}$$

$$k_4 = \frac{s_{11}s_{44}}{s_{11}s_{44}} = 1 \tag{27}$$

Finally, the above equations can be utilized in order to obtain the beam deflection profile of the single-term Galerkin expansion of a square anisotropic CMUT membrane, which is presented in Equation 28.

$$w_{a,1}(x,y) = \left(a^2 - x^2\right)^2\left(a^2 - y^2\right)^2\left(\frac{49\Delta p}{128(7a^4 + 2a^4k_2 + 7a^4k_4)D_a}\right) \tag{28}$$

Similarly, the displacement profile for the three-term Galerkin expansion of a square, anisotropic membrane can be expressed according to Equation 19 to obtain

$$w'_{a,3}(x,y) = \alpha'_{00}\phi'_{00} + \alpha'_{02}\phi'_{02} + \alpha'_{20}\phi'_{20}. \tag{29}$$

The values of α'_{00}, α'_{02}, and α'_{20} where found as described by Thomsen et al [8].

6 Comsol Finite Element Analysis

6.1 FEA Modelling Theory

The finite element analysis (FEA), also known as finite element modelling (FEM), of the electromechanical actuation behaviour of circular and square CMUT devices was performed using the electromechanics module within Comsol, which combines solid mechanics and electrostatics modules with a moving mesh. Specifically, it enables the modelling of linear elastic materials, such as the deformable membrane within a CMUT, using Cauchy's equation, as shown in Equation 30 [9]. In this equation, T corresponds to the stress tensor, which, once solved, is used in order to determine the forces acting upon the dielectric body of the CMUT. This information is exploited by Comsol in a dynamic manner in order to iteratively calculate displacements and the electrostatic forces associated with them.

âĂŐ

$$\rho\frac{d^2r}{dt^2} = \nabla T + f_{ext} \tag{30}$$

6.2 Initial CMUT Comsol Model

Initially a circular, isotropic CMUT was constructed using the 3D space dimension within Comsol and the available Comsol CAD environment. It consists of four distinct materialistic layers: The first layer corresponds to the dynamic membrane, which was grounded, and is comprised of mono-crystalline silicon. The second layer was inserted to simulate the vacuum gap which exists between the two electrodes of the CMUT. The third layer represents a silicon dioxide film which is used in order to prevent pull-in voltage short-circuiting. The final layer corresponds to the biased electrode, which acts as the bulk substrate. It also consists of mono-crystalline silicon. A *finer* mesh configuration, consisting of five vertical elements, was selected for the circular membrane model. The other components of the device design - the air gap, oxide layer, and bottom electrode - were assigned a *coarse* mesh configuration, as these segments do not contribute to the resultant deflection profile of the membrane when the system is unbiased. The completed geometric design of this device is shown in Figure 3.

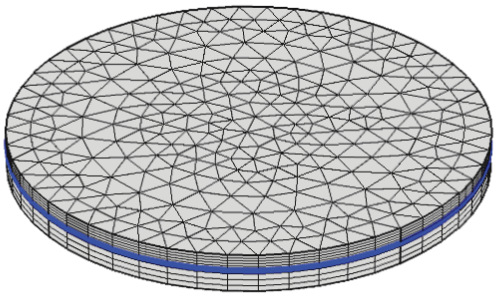

Figure 3: 3D circular CMUT design

The COMSOL simulation of the CMUT in coordination with the Electromechanics *emi* module required meshing, constraining, and voltage boundary conditions. Fixed mesh constraints were applied to the stationary components of the design - namely the biased electrode, the silicon dioxide film, and the circumference of the membrane. Additionally, both electrodes were maintained at 0 V in order to compare the modelled CMUT deflection profile to available analytical solutions to the circular plate equation for constant loads. Lastly, the pressure applied to the topmost section of the membrane was swept parametrically from 0 Pa to 500 kPa in increments of 100 kPa.

6.2.1 Circular CMUT Model Validation

Dimension	Value	Description
Rad	24.5[μm]	Radius of the circular membrane
BotElec	2[μm]	Thickness of the bottom electrode
Oxide	0.21[μm]	Thickness of the oxide layer
Gap	0.37[μm]	Thickness of the vacuum gap
TopElec	1.5[μm]	Thickness of the top electrode

Table 1: Parameter name and default values of circular CMUT membrane model

The validation of this model was performed by comparing the analytical deflection profile of a circular membrane to the numerical solution obtained from the COMSOL model. Equation 12b is used if the center deflection is less than the plate thickness. The device dimensions utilized for this investigation are presented in Table 1 and the graphical comparison between both solutions is shown in Figure 4. Analysis of these figures reveals that the deflection profile of the circular CMUT COMSOL model is in excellent agreement with the analytical solution for a myriad of pressures. Additionally, Figure 4b affirms that these deflection profiles vary linearly as a function of pressure change. This justifies the graphical representation of displacement profiles in reduced units and hence normalized deflection profiles will be used for the remainder of this report.

Following the validation of the circular CMUT model, a model of a square CMUT was constructed and analyzed using FEA.

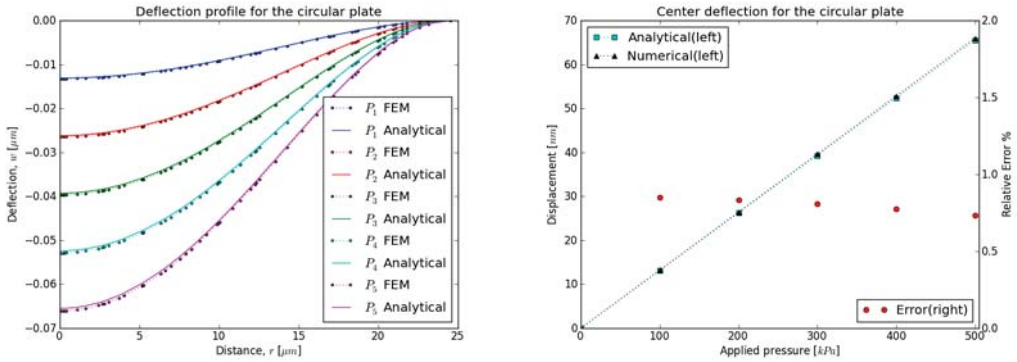

(a) Comparison of analytical deflection profile to Comsol numerical deflection profile

(b) Comparison of analytical peak deflection to Comsol numerical peak deflection

Figure 4: Comparison between analytical and numerical deflection solutions for a circular CMUT design

6.3 Square CMUT Model

The electromechanics module, boundary conditions, as well as the materialistic composition of the circular CMUT model was extended in order to create a Comsol model of a square CMUT. The parameters of this design are displayed in Table 2 and the completed geometric device is shown in Figure 5. An *finer* mesh was selected for the square membrane using an iterative approach and the elaborated procedure is discussed subsequently.

Dimension	Value	Description
EdgeLength	$24.5[\mu m]$	Half the length of the square membrane
BotElec	$2[\mu m]$	Thickness of the bottom electrode
Oxide	$0.21[\mu m]$	Thickness of the oxide layer
Gap	$0.37[\mu m]$	Thickness of the vacuum gap
TopElec	$1.5[\mu m]$	Thickness of the top electrode

Table 2: Parameter name and default values of square CMUT model

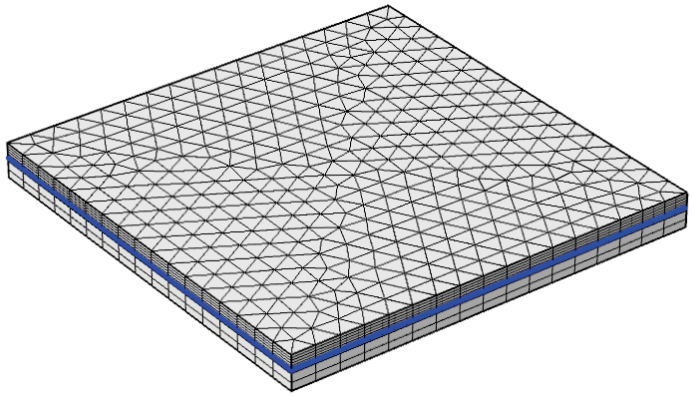

Figure 5: 3D square CMUT design with a *Finer* mesh

6.3.1 Square CMUT Model Validation

By comparing the centre deflection obtained from COMSOL to the expected deflections from Equations 16, 18, and 22. The results are displayed in Figure 6. It can be seen that all the models are in excellent agreement with the obtained numerical result. Thus, it can be concluded that the COMSOL model is correct.

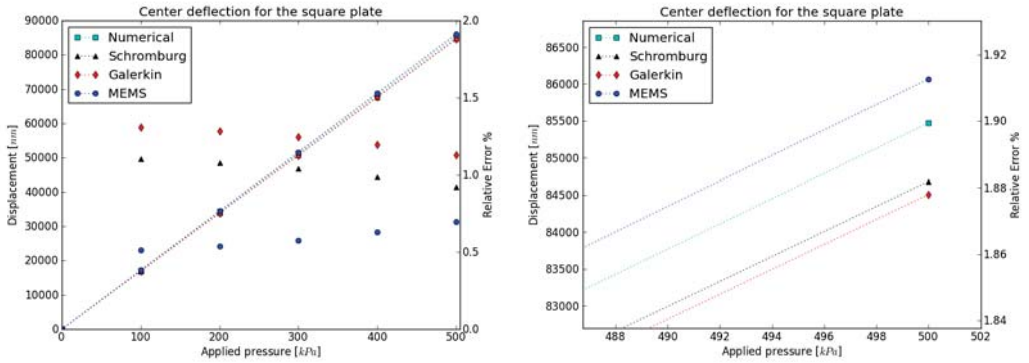

(a) Comparison of analytical centre deflection to the COMSOL numerical deflection

(b) Closer look on the centre deflection of analytical and numerical deflection

Figure 6: Comparison between analytical and numerical center deflection for a square CMUT design

It appears that the MEMS analytical approximation has the best agreement with the FEA model with respect to peak deflection, although all models are considered valid as their respective errors are below 1.5%.

Next, an optimal mesh is obtained for the square membrane using an iterative approach and the elaborated procedure is discussed subsequently.

6.3.2 Square CMUT Mesh Optimization

The mesh of the square CMUT model was optimized by performing a parametric sweep over the bounded pressure values for *normal, fine, finer, extra fine,* and *extremely fine* mesh configurations. The *extremely fine* mesh structure was assumed to correspond to the true membrane displacement profile. Hence the errors of all other mesh arrangements relative to this profile were calculated and the results are presented in Table 3. It was deduced that a mesh profile which yielded a percent relative error below 1.0 % would produce a deflection profile that adequately matches analytical results without hoarding computational resources. Thus, the *finer* mesh configuration was selected as the default profile for the remainder of the COMSOL simulation of the square CMUT design.

Mesh Configuration	Normal	Fine	Finer	Extra Fine	Extremely Fine
% Relative Error	2.3617	1.2373	0.4057	0.0501	0

Table 3: Error of mesh profiles relative to the *extremely fine* configuration

6.4 Model Conversion to Anisotropic Square CMUT

Following the optimization of the isotropic square CMUT model, a duplicate model was constructed. The materialistic composition of the dynamic membrane and bottom electrode of the device were subsequently replaced with [100] mono-crystalline silicon, which is anisotropic by

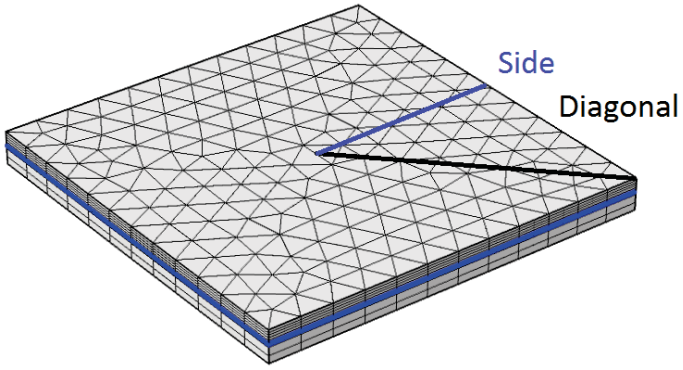

Figure 7: Cut lines along which data was extracted

nature. This alteration required the specification of both compliance and stiffness constants. These values were selected according to Hopcroft [4] and are presented in Equation 6.

This model was then validated by comparing its resultant centre deflection profile to the analytical solutions.

7 Results

The z displacements, referred to as *w2* within the COMSOL environment, where obtained from the FEA model and plotted in a manner such that they could be compared to the macroscopic, microscopic, and Galerkin analytical deflection profiles. One such COMSOL displacement profile is presented in Figure 8. Geometrically, squares contain four symmetry planes and hence two unique symmetry lines were selected - one along the side, the other along the diagonal, as shown in Figure 7.

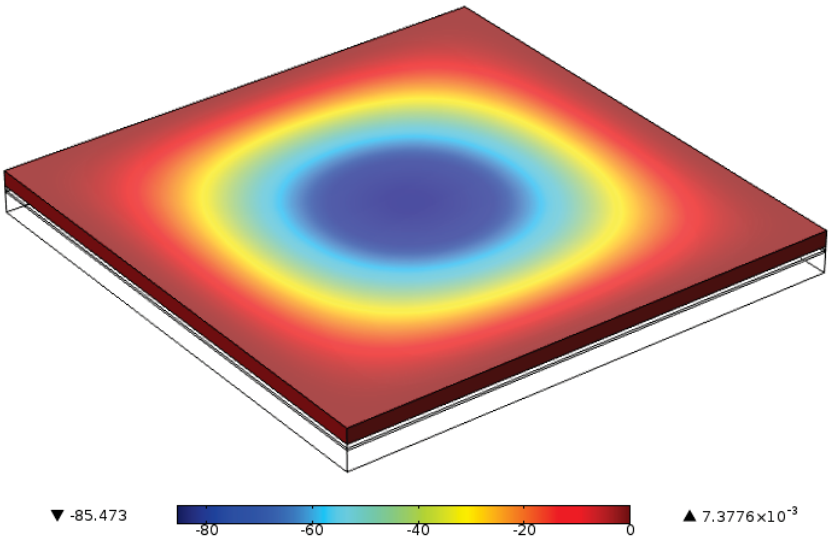

Figure 8: COMSOL deflection profile of a square CMUT

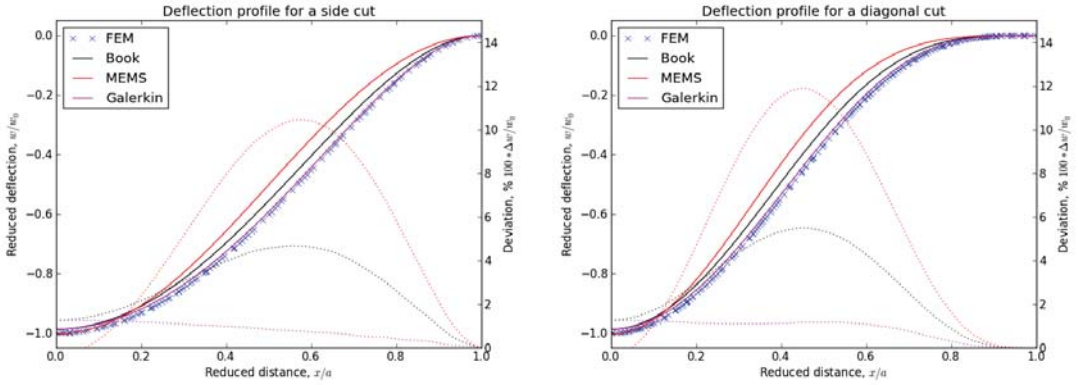

(a) Side deflection profile (b) Diagonal deflection profile

Figure 9: Square isotropic CMUT model comparison for a constant pressure

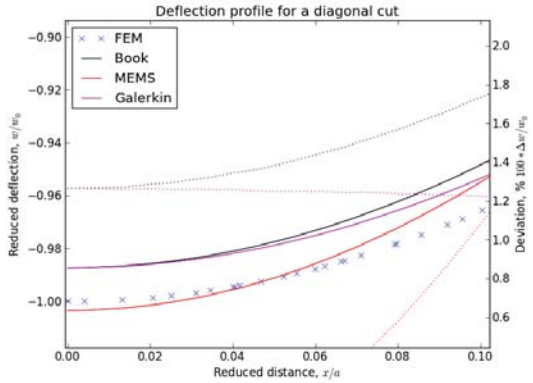

Figure 10: Close up of the center deflection for the diagonal cut from Figure 9b

7.1 Isotropic

The side and diagonal deflection profiles of a square, isotropic CMUT membrane subjected to a constant $P = 100\ kPa$ load are presented in Figure 9. The solid lines within these plots correspond to the analytical deflection profiles. The X line displays the results obtained by FEA model as described above. The dotted lines represent the deviation of the analytical estimation from the FEM results and are plotted with respect to the right axis. A membrane displacement of zero was obtained for the $x = a$ position due to the application of fixed boundary conditions at this point. The point $x = 0$ corresponds to the centre of the membrane and hence where the maximal displacement, w_0, occurs. The plots of the deflection profiles are reduced using w_0 from the FEM results. Evidently, the deflection profile that yields the closest match to the FEM result is that obtained from the Galerkin equation, resulting in a deviation below 2%.

The centre deflection, however, does not match, as shown in Figure 10. This is a consequence of the approximation that was required in order to solve the Garlerkin equation: It is assumed that the plate is thin and hence the aspect ratio (a/h) must be maximized. As the anisotropic square CMUT model consisted of an aspect ratio of ≈ 16.33, such a deviation was expected. Thomsen et al. [8] have shown that for an isotropic plate, a relative difference of 1% is expected for an aspect ratio of 20. Hence the result lies within the acceptable realm of error.

The utilised FEA model does not converge for higher aspect ratios. In order to overcome this issue, each plot can be reduced with respect to its centre deflection, w_0. The resulting deflection profiles are presented in Figure 11 in which the points $x = a$ and $x = 0$ are pinned at 0 and -1,

respectively.

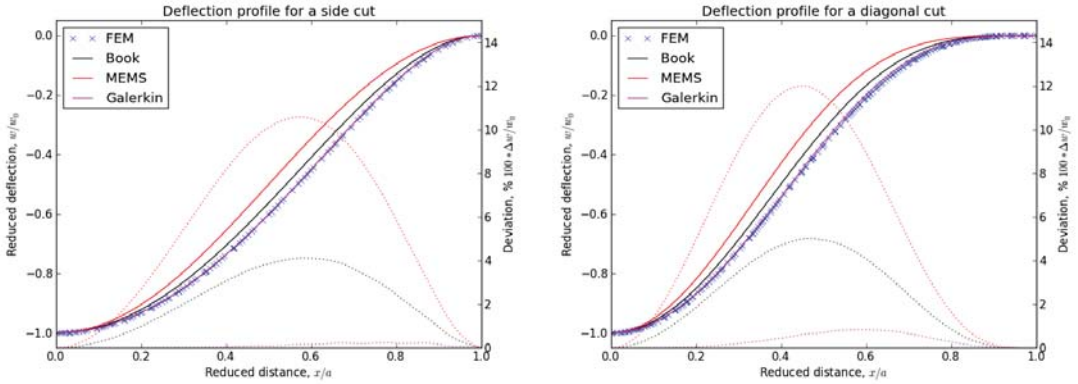

(a) Side deflection profile (b) Diagonal deflection profile

Figure 11: Square isotropic models at the same deflection

This adjustment reveals that the Garlerkin method is in excellent agreement with the FEM results. The deviation of the side deflection profile is below 0.25% and below 0.9% in the case of the diagonal deflection profile.

7.2 Anisotropic

Investigation of the displacement profile of an anisotropic square CMUT membrane yielded equivalent results. With reference to Figure 12, the mismatch in centre deflections between the single-term Galerkin approximation and the FEA model is 5.1% and 0.62% using the tertiary-term expansion. It is expected that a higher-term Galerkin expansion would continue to rapidly converge towards the deflection profile of the FEA model. Hence excellent agreement is obtained between these two approximations.

Again, normalization of each deflection profile with respect to itself enabled the comparison of their shapes with one another. For the single-term Galerkin approximation, the maximal deviation of the side deflection profile occurs at $x = 0$, corresponding to the centre of the CMUT membrane, and was found to be 5.1%. A maximal error of 5.1% was also found for the diagonal deflection profile. For the third-order Galerkin approximation, the maximal deviation of the

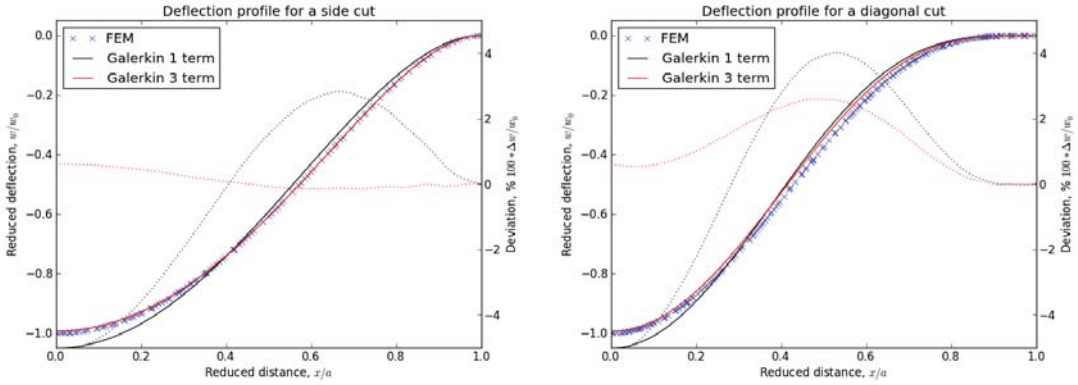

(a) Side deflection profile (b) Diagonal deflection profile

Figure 12: Anisotropic model comparison at constant pressure

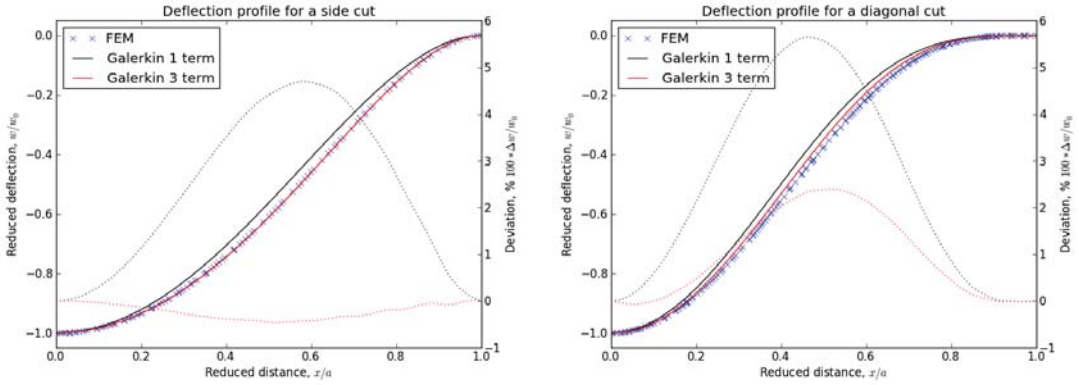

(a) Side deflection profile (b) Diagonal deflection profile

Figure 13: Anisotropic models at the same deflection

side deflection profile occurs at $x = 0$, corresponding to the centre of the CMUT membrane, and was found to be 0.62%. A maximal error of 2.6% was found for the diagonal deflection profile.

The root mean squares of both the deviation of the isotropic and anisotropic models are presented in the Table 4 and 5, respectively.

Table 4: Root mean squares of the deviations of isotropic CMUT model

	Constant Pressure		Constant Center Deflection	
	Side	Diagonal	Side	Diagonal
Macro Approach	2.709	2.854	1.941	2.336
Micro Approach	4.860	5.394	5.001	5.503
Galerkin Method	0.867	0.875	0.077	0.332

Table 5: Root mean squares of the deviations of anisotropic CMUT model

	Constant Pressure		Constant Center Deflection	
	Side	Diagonal	Side	Diagonal
Galerkin, 1 Term	2.465	2.420	2.199	2.607
Galerkin, 3 Terms	0.249	1.295	0.211	1.045

7.3 Pull-In Voltage

Pull-in voltages of the circular and square membrane of the same width where iteratively determined. It can be seen that the pull-in voltage of the circular membrane is much lower than the square membrane, potentially due to symmetry. Thus less force is required to collapse the membrane.

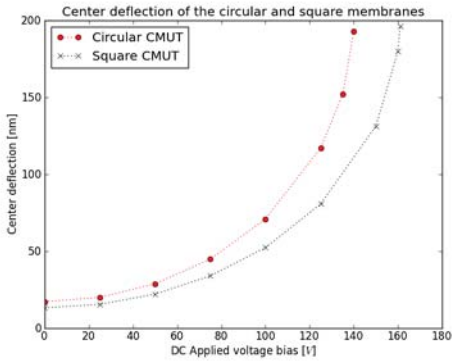

Figure 14: Pull-in voltage of the square and circular membrane CMUT, using values defined in Table 1

8 Conclusions

A Comsol FEM analysis of a square CMUT was performed. The lack of a closed-form analytical solution to such a model required the validation of the utilized boundary conditions by first simulating a circular model. The circular model was found to be in good agreement with available analytical solutions. Hence the employed, validated boundary conditions were used in the construction of both isotropic and anisotropic square CMUTs. The deflection profile of the isotropic square CMUT was compared to two commonly accepted models as well as the Galerkin model proposed by Thomsen et al. This comparison revealed that the FEM results were in excellent agreement with these analytical models. The lowest error, relative to the FEA simulation, was obtained through the use of the Galerkin method, which resulted in an average error below 1% without correction. Following the correction of the centre deflection, which arose due to the selected aspect ratio, a maximum error below 1% is obtained. The Galerkin method was also employed in the estimation of the deflection profile of the anisotropic case. The other analytical models used in the investigation of isotropic electrodes cannot be extended to the study of anisotropic materials. It was found that the Galerkin method is in excellent agreement with the FEA simulation and converges equally well for both isotropic and anisotropic cases. An error of less than 2.5% was obtained using the three-term Galerkin expansion.

References

[1] G. Treece, "F-gmt11-1: Ultrasound beamforming simulator," Jan 2005.

[2] M. Najar, "Design and analysis of capacitive micromachined ultrasound transducer," Master's thesis, University of British Columbia, September 2010.

[3] X. Jin, I. Ladabaum, F. Degertekin, S. Calmes, and B. Khuri-Yakub, "Fabrication and characterization of surface micromachined capacitive ultrasonic immersion transducers," *Microelectromechanical Systems, Journal of*, vol. 8, pp. 100 –114, mar 1999.

[4] M. Hopcroft, W. Nix, and T. Kenny, "What is the young's modulus of silicon?," *Microelectromechanical Systems, Journal of*, vol. 19, pp. 229 –238, april 2010.

[5] Y. Huang, A. Ergun, E. Haeggstrom, M. Badi, and B. Khuri-Yakub, "Fabricating capacitive micromachined ultrasonic transducers with wafer-bonding technology," *Microelectromechanical Systems, Journal of*, vol. 12, pp. 128 – 137, apr 2003.

[6] W. K. Schomburg, "Membranes," in *Introduction to Microsystem Design*, vol. 1 of *RWTHedition*, pp. 29–52, Springer Berlin Heidelberg, 2011.

[7] O. Hansen, "Lesson 13: Energy methods." Lecture Notes, September 2012. 33355 MEMS 2.

[8] E. Thomsen, K. Reck, G. Skands, C. Bertelsen, and O. Hansen, "Silicon as an anisotropic mechanical material bending of thin crysralline plates," unpublished work, Danmarks Tekniske Universitet, September 2012. 33355 MEMS 2.

[9] C. Multiphysics, "Comsol help file: The electromechanics interface." Help Files, September 2012. 33355 MEMS 2.